Indian Journal of Chemistry
Vol. 64, February 2025, pp. 192-212
DOI: 10.56042/ijc.v64i2.15354

Molecular docking and dynamic simulation of phytochemical components from *Clitoria ternatea* against different hormone-dependent cancer cell lines

Fouzi S Aboud*[a,b], Majed A Al-Shaeri[a], Ali T Zari[a,e,f], Ehab M Ali[c,d] & Naif A Almalki[c,g]

[a] Department of Biological Sciences, Faculty of Science, King Abdulaziz University, Jeddah 21589, Saudi Arabia

[b] Department of Anatomy, Histology and Embryology, Faculty of Medicine, University of Tripoli, Tripoli 13932, Libya

[c] Department of Biochemistry, Faculty of Science, King Abdulaziz University, Jeddah 21589, Saudi Arabia

[d] Department of Chemistry, Faculty of Science, Tanta University, Tanta 3152, Egypt

[e] Centre of Excellence in Bionanoscience, King Abdulaziz University, Jeddah, Saudi Arabia

[f] Princess Dr. Najla Bint Saud Al-Saud Centre for Excellence Research in Biotechnology, King Abdulaziz University, Jeddah, Saudi Arabia

[g] Experimental Biochemistry Unit, King Fahd Medical Research Centre, King Abdulaziz University, Jeddah, Saudi Arabia

Email: fmiftah@stu.kau.edu.sa

Received 28 November 2024; accepted (revised) 22 January 2025

Creating novel non-toxic drug candidates targeting breast cancer (BC) cells with no effects on normal cells is at the top of research objectives. Blue *Clitoria ternatea* (*C. ternatea*) flowers were macerated in ethanol and evaporated using a precision economy incubator at 40°C to isolate the major phytochemical compounds. The GC-MS technique was used to identify the chemical structure of isolated components. Molecular docking, molecular dynamic simulation, and pharmacokinetics analytical tools were used to measure the binding affinity, stability, and solubility degree of isolated compounds bound to caspase-3. Normal HSF and different BC cell lines were grown for 24 h and 48 h to evaluate antiproliferative and caspase-3 activity against the metastatic BC cell line (of interest) MDA-MB-231. Computational analysis of compound 4CT: CID-22212496 (Cholesta-8,24-dien-3-ol) showed poor solubility, stable binding affinity (–7.6 kcal/mol), and strong interactions across several amino acid residues. Antiproliferative experiments showed no toxic activities of isolated compounds on cell growth of the normal cell line HSF with a IC_{50} value of 869.6±5.04 µg/mL compared to cells treated with DOX following 24 h. In contrast, significant inhibition of cell viability was observed, particularly in the BC cell line MDA-MB-231, with IC_{50} values of 363.06±6.94 µg/mL and 209.4±4.06 µg/mL following 24 h and 48 h, respectively, with increased levels of caspase-3 enzyme (*p-value* < 0.001). We suggest that the Cholesta-8,24-dien-3-ol compound may have potential anticancer activity by blocking the estrogen receptor and consequently inhibiting estrogen biosynthesis through the activation of the intrinsic caspase-3 pathway.

Keywords: Blue tea flowers, Caspase-3, Cholesta-8,24-dien-3, Cytotoxicity, Pharmacokinetics, Metastatic TNBC cells

Cancer has been viewed for many decades as a severe illness that affects human life and has played a role in numerous human fatalities for people under the age of 70[1]. Breast cancer (BC) is considered the most prevalent and has the highest incidence among women. Most breast malignancies are carcinomas and classified on their degree of invasiveness, pathological features, and hormonal expression into four categories based on molecular subtyping: luminal type A (ER^+, $PR^\pm$, $HER2^-$), luminal type B (ER^+, $PR^\pm$, $HER2^\pm$), human epidermal growth factor receptor 2 (ER^-, PR^-, $HER2^+$), and triple-negative breast cancer (TNBC) (ER^-, PR^-, and $HER2^-$)[2].

The molecular subtype, TNBC, is thought to be the most aggressive type of BC; it does not express any hormonal receptors. It can be further divided into six subclasses: immune modulator, mesenchymal, stem-like mesenchymal, basal-like (BL1 and BL2), luminal androgen receptor subtype, and mesenchymal[3]. Although ERα is absent in TNBC, this subtype can exhibit estrogen-responsivity when ERβ and G protein-coupled estrogen receptor 1 (GPER-1) are expressed. Constitutively active estrogen-related receptors (ERRs) can also activate and modify estrogen signaling pathways in TNBC[4].

Medicinal plants have a curative value as biologically active ingredients of the primary and secondary metabolites are obtained either in pure or combined form, with little side effects and cost-effectiveness compared to expensive synthetic

medications[5]. The species, *C. ternatea*, which is also known as Asian pigeon wings or butterfly pea, is marketed under the name Bunga telang. It is a perennial creeping herbal plant that belongs to the *Fabaceae* family and has drawn a lot of attention in medical applications. Previous studies have demonstrated that distinct plant sections have varying secondary metabolites, such as alkaloids and flavonoids[6] that showed promising therapeutic effects as antimicrobial and anticancer agents[7,8].

However, phenolic acids are natural phytochemical compounds, classified into simple and complex compounds that are found extensively in fruits and vegetables[9]. For instance, benzoic acid compounds are a class of simple phenolic acids that have shown potent anticancer activities, inhibiting cancer cell growth, angiogenesis, and invasion[10–12].

The apoptosis mechanism is a complicated set of morphological changes, including nuclear condensation, fragmentation, plasma membrane blebbing, and generating apoptotic bodies to sustain the regular turnover of cells and embryonic development[13]. One of the most effective enzymes is caspase-3, which is required for the process of apoptosis[14]. For instance, neurological illnesses, ischemic damage, autoimmune diseases, and cancer can be caused by changes to the normal apoptotic pathway[15]. The process of apoptosis in cancer cells *via* intrinsic or extrinsic pathways through induction of mitochondrial membrane potential is the focus of many prospective therapeutic approaches against cell survival or proliferation processes as well as the tumor microenvironment[16].

Computational analytical techniques such as molecular docking and dynamics are recently used for understanding drug behavior. It is based on the binding between ligands and specific proteins to make certain interactions[17]. In our design study, molecular docking, dynamic simulation, and pharmacokinetic analysis were employed in combination with *in vitro* experiments to evaluate the stability and cytotoxic activities of isolated blue *C. Ternatea* flowers organic compounds on different BC cell lines, which may develop as promising drug candidates against hormone-dependent cancers.

Materials and methods

Chemical and reagents

The materials used in this study including Ethanol (Sigma-Aldrich®), Dulbecco's Modified Eagle Medium (DMEM) (Hyclone®), Dulbecco's Phosphate Buffered Saline (DPBS) (Hyclone®) FetalBovine Serum (FBS) (Hyclone®), Trypsin-EDTA (Hyclone®), Dimethyl Sulphoxide (DMSO) (Sigma-Aldrich®), Doxorubicin (DOX) (SWISS PARENTERALS LTD®), MTT cell growth assay kit (Sigma Aldrich®), and Caspase-Glo assay Kit (Promega®).

Equipment and software

The equipment used in the experiments was Milli Q water (MILLIPORE SAS®), a digital orbital shaker (DAIH-SCIENTIFIC®), precision economy incubator (Thermo-Fisher Scientific®), ultraviolet-visible (UV-VIS) spectrophotometer (Bibby Scientific®), Fourier-transfer infrared (FTIR) spectroscopy (Thermo-Fisher Scientific®), gas chromatograph mass spectrometer (GC-MS) (Agilent®), and microplate reader (Agilent®). The software used for molecular dynamic, and simulation was Research Collaboratory for Structural Bioinformatics–Protein Data Bank (RCSB-PDB), BIOVIA Discovery Studio, PyMOL 2.5.0. CASTp, PyRx – Virtual Screening Tools program, PubChem, Microsoft Excel 2016, GROMACS, CHARMM General Force Field (CGenFF) server, and DiffDock software.

Plant collection and identification

The fresh flowers of *C. ternatea* were collected from Yanbu governorate in Radwa Mountain, western region of Al-Madinah Al-Munawwara, Saudi Arabia. The sample was classified and authenticated by a plant taxonomist at the Department of Biology, KAU, with sample voucher CT18004.

Plant extract preparation

A pure ethanolic crude extract from *C. ternatea* flowers was prepared according to the method of Bennour *et al.*[18]. The flowers were thoroughly washed with Milli Q water (MILLIPORE SAS®) to stick dirt particles, then were air-dried at room temperature for 21 days. The dried flowers were pulverized using a mechanical grinder until a soft powder was obtained and kept in an airtight container in a dry place. A known weight of dried powdered flowers (25 g) was added to 250 mL of 80% ethanol (Sigma-Aldrich®) and macerated for 72 h with a digital orbital shaker (DAIH-SCIENTIFIC®). The extracted solution was filtered with Whatman No. 1 filter paper, and the filtrate was evaporated in the dark using a precision economy incubator (Thermo-Fisher Scientific®) at 40°C for 2 h until a dry extract was obtained, stored at 20°C, and used prior to the experiments.

Tri-spectroscopy screening of ethoxy extract

A UV-VIS spectrophotometer (Bibby Scientific®) was used to identify the main band patterns. The *C. ternatea* extract was examined under UV-VIS light at wavelengths ranging from 200 to 800 nm using the same solvent at a 1:10 ratio[19].

To identify the main functional groups in the ethanolic extraction of *C. ternatea*, a small amount of the extract was placed on a sample holder. Absorbance and transparent analysis were then performed using FTIR spectroscopy (Thermo-Fisher Scientific®), which were scanned from 4000 to 500 cm^{-1}[20,21].

The bioactive compounds of *C. ternatea* were isolated using a capillary column GC-MS (Agilent ®), by injecting the samples into the spectrometer using split mode and a 300°C injection port temperature setting. The flow of helium was 1.61 ml/min at 280°C. The temperature increased by approximately 10°C per minute after reaching 50°C in the first minute, eventually reaching 300°C. The scan mode was conducted for a total of 32 min, covering a 40–500 m/z range. The molecules were then identified using the mass spectral database NIST~98[22].

Protein preparation

Three-dimensional (3D) structure of caspase-3 (1GFW) was downloaded from the RCSB-PDB (https://www.rcsb.org) in PDB format. After that, the protein was accoutred and defected by removing side chains, water, and hetatm using BIOVIA Discovery Studio and PyMOL 2.5.0 software as shown in Fig. 1.

Ligand preparation

The chemical structure of isolated compounds from *C. ternatea* was downloaded from PubChem website server: https://www.pubchem.ncbi.nlm.nih.gov/. These structures were then processed and prepared using Auto-Dock Vina and PyRx—virtual screening software to determine the binding affinity.

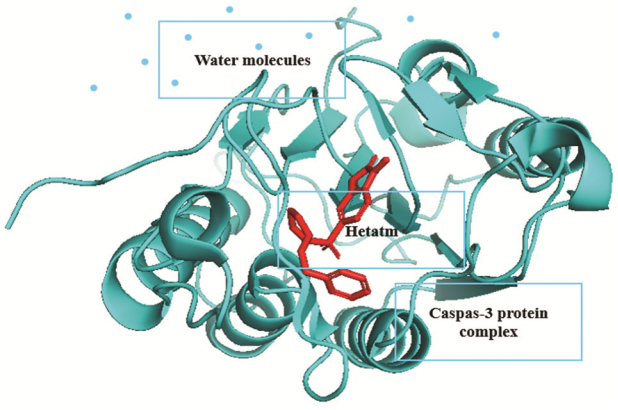

Fig. 1 — GCMS analysis of pure ethanolic extract of C. ternate flowers.

Generating of receptor grid

A grid was created in Glide with a default Van der Waals radius scaling factor of 1.0 and a charge cutoff of 0.25. The minimized structure was then exposed to the OPLS_2005 force field. The ligand active site was surrounded by a cubic box, fitted to 14 × 14 × 14 for docking the ligands with 1 GFW protein one by one[23].

Computational pharmacokinetics

ADMET, which categorizes pharmaceuticals based on absorption, distribution, metabolism, excretion, and toxicity, provides the best description of the relationship between medication dosages and their concentration over time. When selecting a chemical for potential therapy, we first examine its analogs by carefully choosing compounds that can affect both *in vivo* and *in vitro* experimental outcomes. Swiss-ADME is an online program available at http://www.swissadme.ch/index.php. that assesses a compound's solubility, bioavailability, and toxicity to identify potentially beneficial options. Furthermore, the safety profiles of the compounds were evaluated using computer-aided design and drafting.

Molecular Dynamic (MD) simulation

The molecular dynamic (MD) simulations were conducted using GROMACS. The protein structure (1GFW) was obtained from the RCSB-PDB, and the ligand parameters were determined using the CHARMM General Force Field (CGenFF) server, which provided files containing the topologies for all compounds. The protein was modeled using the CHARMM36 force field, while the ligands were parameterized with CGenFF[24]. The system was then solved in a cubic box filled with TIP3P water molecules and counterions to neutralize the overall charge of the system.

Energy minimization was performed using the steepest descent algorithm to eliminate any steric clashes or unfavorable contacts within the system. Minimization was further continued until the maximum force on any atom fell below 1000 kJ/mol/nm to ensure that a sufficiently stable starting conformation existed for the subsequent simulation steps. After the minimization, the system was further equilibrated in two steps: first, a 100 ps NVT

equilibration, where the temperature is set to 300 K and stabilized using a modified Berendsen thermostat. The second phase was 100 ps NPT equilibration to stabilize the pressure at 1 bar using a Parrinello-Rahman barostat with heavy atoms of the protein and ligand constrained for both phases[25].

A total of 100 ns production MD under the NPT condition was performed free from restraints. The LINCS algorithm constrained bond lengths, with a time step of 2 fs. The search for neighbours used the Verlet cut off scheme and a 1.2 nm cut off for non-bonded interactions. Long-range electrostatic interaction was described using the particle mesh Ewald (PME) method of Abraham *et al*.[26].

Experimental section

Stock solution and cell culture preparations

The obtained extract from *C. tenatea* was diluted by each 10 mg in 1 ml of DMSO (Sigma-Aldrich®). From stock (20 mg) of DOX (SWISS PARENTERALS LTD®), 2.5 µL was added to 2 mL of media to prepare a 50 µg/mL concentration. The normal cell line human skin fibroblasts (HSF) and the BC cell lines MCF-7, T47D, and MDA-MB-231 were obtained from King Fahd Medical Research Centre (KFMRC), Jeddah, Saudi Arabia.

All the experimental cells were grown separately in filtered flasks containing 2 mL of DMEM (Hyclone®), 10% FBS, and 1% penicillin-streptomycin antibiotics (Hyclone®), and incubated under a humidifying atmosphere containing 5% CO_2 and 95% air at 37°C under strict sterilize conditions. The cells were sub-cultured for 3-4 days by washing the monolayers with PBS (Hyclone®), followed by a brief incubation with trypsin. The cells growing at the exponential phase were used to perform the experiments.

Antiproliferative assay

The MTT cell viability assay was performed according to Kamiloglu *et al.*[27] by dissolving 5 mg/mL of MTT (3-[4,5-dimethylthiazol-2-yl]-2,5-diphenyltetrazolium bromide) in Dulbecco's Phosphate Buffered Saline (DPBS, *p*H 7.4). After that, the MTT solution was filtered through a 0.2 µM filter into a sterile, light-protected container prior to the testing. The experimental cell lines HSF, MCF-7, T47D, and MDA-MB-231 were seeded at a density of 1×10^4 cells per well of 96-well plates in 200 µL of culture medium.

Normal cell line HSF was treated with various concentrations of DOX in the range of 1.56-25 µg/mL and *C. ternatea* extract in the range of 50-800 µg/mL for 24 h to evaluate the acute toxicity of isolated compounds; the BC cell lines were treated with DOX in the range of 0.75-12.5 µg/mL and *C. ternatea* extract in the range of 50-800 µg/mL for 24 h and 48 h to evaluate the anticancer activity of isolated compounds.

Following 24 h and 48 h treatment, 10 µL of MTT (Sigma-Aldrich®), was added to each cell well and incubated for 3 h at 37°C. After that, the formazan product produced by treated cells was dissolved using 100 µL of DMSO by gradually rotating the plates for 10 min. The microplate reader was used to measure the vitality of the cells at 490 nm.

Selectivity index calculation

The ratio of sample toxicity concentration to its effective bioactive concentration is known as the selectivity index (SI). The optimal medication should have very low active concentration and relatively high toxic concentration. The equation of SI was applied on all experimental cells by dividing the IC_{50}value of non-malignant cells (normal cells) by the IC_{50} value of malignant cells. Generally, the ratio of SI ranges between 1.96 and 51.3 was considered significant[28].

$$SI = \frac{IC_{50}^{\text{Non-Malignant cells}}}{IC_{50}^{\text{Maligant cells}}}$$

Microscopical examination

The morphology of cultured normal cells (HSF) was examined under a microscope after 24 h of treatment to evaluate the acute toxicity of isolated compounds. For BC cells MCF-7, T47D, and MDA-MB-231, a microscopical examination was done following 24 h and 48 h of treatment using a 12.5-megapixel digital camera (Leica®); photos of the cells were taken to analyze how the treatments affected the morphology of the cells.

Caspase-3 activity assay

Caspase activity was measured using the Caspase-Glo Assay Kit (Promega®). The BC cell line (of interest) was seeded, grown, and treated with various concentrations of DOX (1.5 µg/mL, 3 µg/mL, and 6 µg/mL) and *C. terantea* extract (50 µg/mL, 100 µg/mL, and 200 µg/mL). CASPASE-GLO 3 reagent was added without removing the medium from the wells and incubated for 3 h at room temperature; luminescence was measured using a microplate reader.

Results

Phytochemical analysis

The UV-VIS spectra of the ethoxy extraction of *C. ternatea* flowers showed different band patterns in three clusters. The results of UV-VIS cluster bands were summarized in Table 1 and Fig. 2a. FTIR spectra was used to identify the functional groups of the active components present in the extract based on the peak's values in the region of infrared radiation. The results of FTIR peak intensities and functional groups were represented in Table 2. It was clear that the number of phenolic and/or alcohol (O-H) gave a broad peak at around 3310-3370 cm^{-1}. The aromatic rings (C=C) and amine (N-H) groups at the peak of 1610-1650 cm^{-1} as shown in Fig. 2b. In total, 13 different compounds are isolated from *C. ternatea* through the GC-MS. Gas chromatography spectrum showed different major components with peak intensity characterized majorly by the presence of the phenolics, aromatic organic compounds, and esters.

Table 1 — UV-VIS spectrophotometry characterization of ethoxy *C. ternatea* extraction

Sample	Wavelength (nm)	Absorbance	Functional groups
C. ternatea	221	3.7	Double bonds (Olefinic and aromatic compounds)
	266	1.95	Double bonds (Olefinic and aromatic compounds)
	302	1.21	Non-bonding electrons in (C=O) and (O=C-OH) groups
	352	1.25	Aromatic compounds

Table 2 — FTIR spectra characterization of ethoxy *C. terantea* flowers extraction

Sample	Wave number (cm^{-1})	Intensity	Bond responsible
	3310	1.64	ν:O-H (Phenolic, Alcohol
	2930	0.85	ν:C-H (Methyl & Methylene)
	1710	1.04	ν:C=O (Ester)
	1620	1.17	ν:C=C (Aromatic rings); δ: N-H (Amine)
C. ternatea	1420	0.93	δ:C-H (Saccharides)
	1370	1.09	δ:C-H (Ester)
	1230	0.75	ν:C-O (Ester, glycoside)
	1060	1.99	ν:C-O (Alcohol, acid, Saccharides)

(ν: stretching; δ: bending)

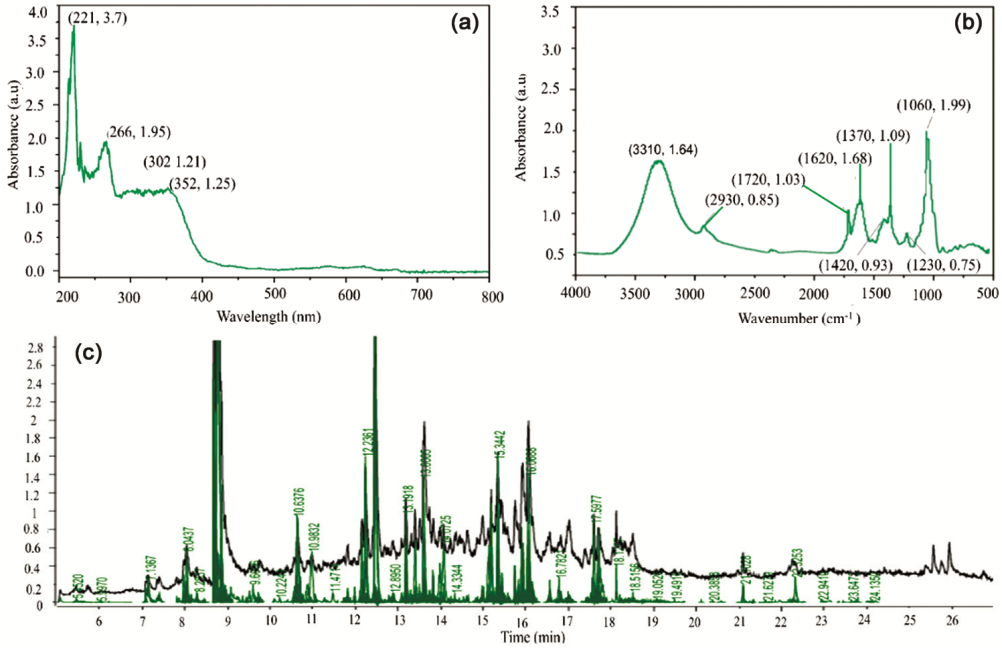

Fig. 2 — Molecular docking of selected compounds: (a) 3-Oxatricyclo-triaconta, (b)Methyl-piperidin-1-yl, (c)Piperidin-benzo[de] isoquinolin-2-yl)-propionic acid-, and (d) cholesta-8,24-dien-3-ol, with (e) targeted receptor 1GFW.

Novel phytochemical components of phenyl-amino-benzoic acid compounds were identified in *C. ternatea* flower samples between 8.0 and 26.0 min within the assays, as displayed in Table 3 and Fig. 2c

MD analysis

The active protein binding sites were identified using the PyMOL server. The targeted receptor exhibited binding sites mainly at the positions of ARG 207, CYS 163, GLU 122, SER 120, SER 205, TYR 204, MET 61, HIS 121, PHE 250, and TRP 206 at three short distances: 2.6 Å, 3.0 Å, and 3.3 Å, as presented in Table 4 and shown in Fig. 3. The PyRx tools and Auto-Dock Vina were used to dock the *C. ternatea* compounds with the 1GFW receptor and give binding affinity values between –3.1 and –8.9. The compounds that showed the highest binding scores were selected as shown in Table 5 and Fig. 4.

The auto-dock of four selected compounds with caspase-3 revealed various bonding interactions. In compound CID-5368332, hydrophobic bonds were observed at the positions TYR-204, TRP-206, and PHE-252 with distances of 5.33 Å, 4.73 Å, and 4.97 Å, respectively, and one hydrogen bond at position of

Table 3 — GC-MS analysis of ethoxy *C. terantea* flowers extraction

Peak	Retention time	Compounds	Formula	Area	Percentages
1	8.2089	1,3-Dioxo-6-piperidin-benzo[de] isoquinolin-2-yl)-propionic acid-	$C_{20}H_{20}N_2O_4$	1278178.3	66.8
2	8.2913	2-Methyl-4-phenoxy-5,6-diphenyl-2H-pyridazin-3-1	$C_{23}H_{18}N_2O_2$	264771.8	50.4
3	8.5188	(4-Methyl-piperidin-1-yl)-acetic acid, (2-oxo-2,3-dihydro-benzo [e]indol-1	$C_{20}H_{22}N_4O_2$	161685.7	60.2
4	11.5344	1,3-Benzenediol, o-(3-methylbut-2-enoyl)-o'-(2-fluorobenzoyl)-	$C_{18}H_{15}FO_4$	1573019.0	52.7
5	16.8192	1H-Imidazole-5-carboxamide, 4-amino-1-methyl-N-(4-phenoxyphenyl)-	$C_{17}H_{16}N_4O_2$	821608.8	50.9
6	16.8883	Carbamic acid, 2-methoxy-4-tetrahydro-2-furanyl) carbonyl-amino-phenyl	$C_{15}H_{20}N_2O_5$	3600749.8	59.8
7	17.0189	Benzenemethanamine, alpha. -(2-imino-1-methyl-2-phenyl ethylidene)-N-phenyl-	$C_{22}H_{20}N_2$	4708995.8	52.3
8	17.0266	2-(4-Methoxyphenyl)-8-chloro-4H-imidazo(2,1-c) (1,4) benzoxazine	$C_{17}H_{13}ClN_2O_2$	1442749.7	51.0
9	17.0494	1H-Benzoimidazole, 1-(4-fluoro benzyl)-2-(thiophen-2-yl)-	$C_{18}H_{13}FN_2S$	2335001.3	50.3
10	18.8096	1H-Indole-3-acetamide, N-(1,3-benzodioxol-5-ylmethyl)-2-methyl	$C_{19}H_{16}N_2O_4$	10232760.9	50.7
11	21.1829	2-Benzofurancarboxylic acid, 7-methoxy-, (3,4,4-trimethyl-1,2-dioxetan-3-yl)	$C_{16}H_{18}O_6$	2315422.1	56.0
12	25.9425	Cholesta-8,24-dien-3-ol, 4-methyl-, (3.beta.,4.alpha.)-	$C_{28}H_{46}O$	156237724.3	55.7
13	26.5341	3-Oxatricyclo [20.8.0.0 (7,16)] triaconta-1(22),7 (16),9,13,23,29-hexaene	$C_{29}H_{42}O$	91604282.8	50.3

Table 4 — Active prediction of targeted protein caspase-3

Protein	volume (SA)	Area (SA)	Resolution	Total AA residue in chain A	AA residue at predictive active site
Caspase-3	64.032	82.180	1.75	147	29

(SA: Surface Area; AA: Amino Acid)

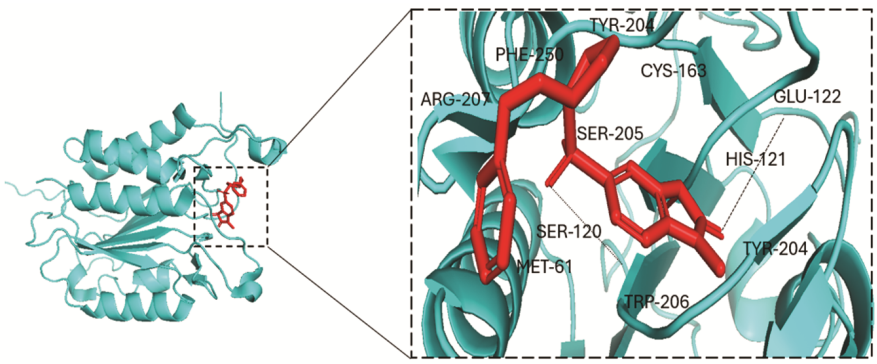

Fig. 3 — Graphical representation of molecular dynamics simulations showing RMS of ligand-protein complex over 100 ns period of simulations for four selected compounds.

Table 5 — Docking scores of isolated compounds from the *C. ternatea* flowers

S. No.	Chemical name	Pub Chem ID	Molecular Formula	Molecular Weight	Binding Affinity
1	3-Oxatricyclo-triaconta	CID5368332	$C_{29}H4_2O$	406.6 g/mol	–8.9 Kcal/mol
2	4-Methyl-piperidin-1-yl)- acetic-acid-2,3-dihydro- benzo[e]indol-1	CID135592970	$C_{20}H_{22}N_4O_2$	350.4 g/mol	–8.1 Kcal/mol
3	Piperidin-benzo[de]- isoquinolin-2-yl)-propionic acid-	CID6426095	$C_{20}H_{20}N_2O_4$	518.4 g/mol	–7.9 Kcal/mol
4	Cholesta-8,24-dien-3-ol	CID22212496	$C_{28}H_{46}O$	398.7 g/mol	–7.6 Kcal/mol

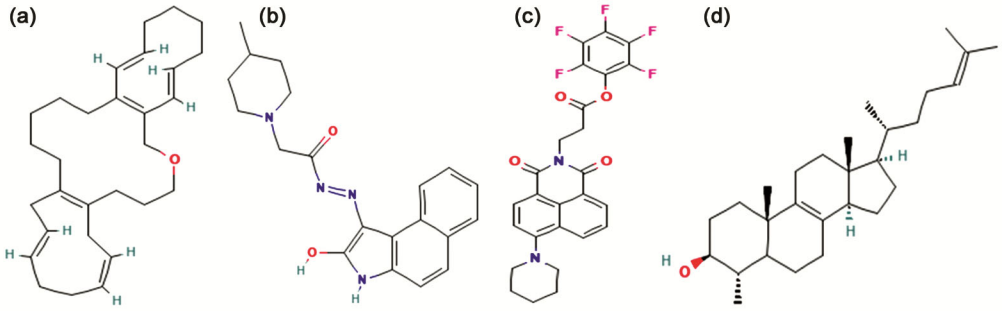

Fig. 4 — Graphical representation of molecular dynamics simulations showing RMD of ligand-protein complex over 100 ns period of simulations for four selected compounds.

SER251 with 2.97 Å (Fig. 5a & b). In contrast, several hydrogen bonds were demonstrated in the compound CID-135592970 at the positions SER-251, PHE-250, and ASN-208 with least distances of 2.19 Å, 2.46 Å, and 3.11 Å, respectively (Fig. 5c & d). For compound CID-6426095, hydrogen bonds were found at ARG-207 at many distances of 2.80 Å, 3.30 Å, 3.17 Å, and 3.39 Å and one halogen bond at the positions of SER-63 with a distance 3.53 Å (Fig. 5e & f). The fourth compound, CID- 22212496 showed hydrogen bonds at the positions CYS-163 and ARG-207 with distances of 3.76 Å and 3.25 Å, respectively. Hydrophobic bonds were detected at the positions PHE-256 and TYR-204 with distances of 5.17 Å and 4.29 Å and 4.85 Å, respectively (Fig. 5g & h).

ADMET analysis

According to Lipinski's rule[29], which limits molecular weight (MW) to < 500 g/mol, most of selected compounds from *C. Ternatea* (1CT, 2CT, 3CT, and 4CT) showed ideal MW values within the recommended ranges, except for compound 3 that showed high MW > 500 g/mol. The hydrogen bond donors (HBD) increase acidity, which should be (< 5), while the hydrogen bond acceptor (HBA) increases basicity, which should be (< 10)[30]. We found that all the compounds possess well-qualified bonding. Log P represents the compound's lipophilicity; the recommended range should be within (-2.0-6.5) to be accepted and exhibit good oral absorption. For compounds 1CT, 3CT, and 4CT, Log P was above the recommended value of 6.5, indicating high lipophilicity[31]. Log S is the aqueous solubility of compounds that directly influence oral absorption, which should be within (-6.5-0.6). For compounds 1CT, 2CT, 3CT and 4CT, poor solubility was detected with values more than –6.5, with lower gastrointestinal (GI) absorption was demonstrated in compounds 1CT and 4CT. Finally, all the selected compounds were unable to cross the blood-brain barrier (BBB) and have no cytotoxic activity[30], as presented in Table 6.

MD simulation analysis

Root Mean Square Deviation (RMSD) analysis

The Root Mean Square Deviation (RMSD) graph provides valuable insights into the dynamic stability of caspase-3 when bound to four different ligands over a 100-nanosecond simulation. In compound CID-5368332, the RMSD remains relatively stable for the first 60 nanoseconds at around 1 nm; after that, there is a dramatic increase in RMSD, reaching up to 5 nm, indicating unstable interaction with caspase-3 leading to the protein's structural deviation. Compounds CID-135592970 and CID-6426095 showed a stable interaction with RMSD remaining around 1 nm, indicating relative stability. In contrast, compound CID-22212496 displays the most stable RMSD profile across the entire simulation. It fluctuates minimally, staying within the 0.5 to 0.75

nm range throughout the 100 ns, as shown in Fig. 6a. This low deviation indicates a highly stable interaction between the compound and caspase-3.

Root Mean Square Fluctuation (RMSF) analysis

The Root Mean Square Fluctuation (RMSF) helps in understanding how flexible or rigid each residue of the protein is during the simulation over a 100-nanosecond simulation. The protein complex with compound CID-5368332 exhibited moderate fluctuations across most of the residues, remaining below 0.5 nm for most of the protein. There is a noticeable spike at the very end near residue 180, where the fluctuation reaches around 3.5 nm, indicating instability of this compound. For compounds CID-135592970 and CID-6426095, they showed low fluctuations below 0.5 nm. There was a sharp increase in fluctuation towards the C-terminal

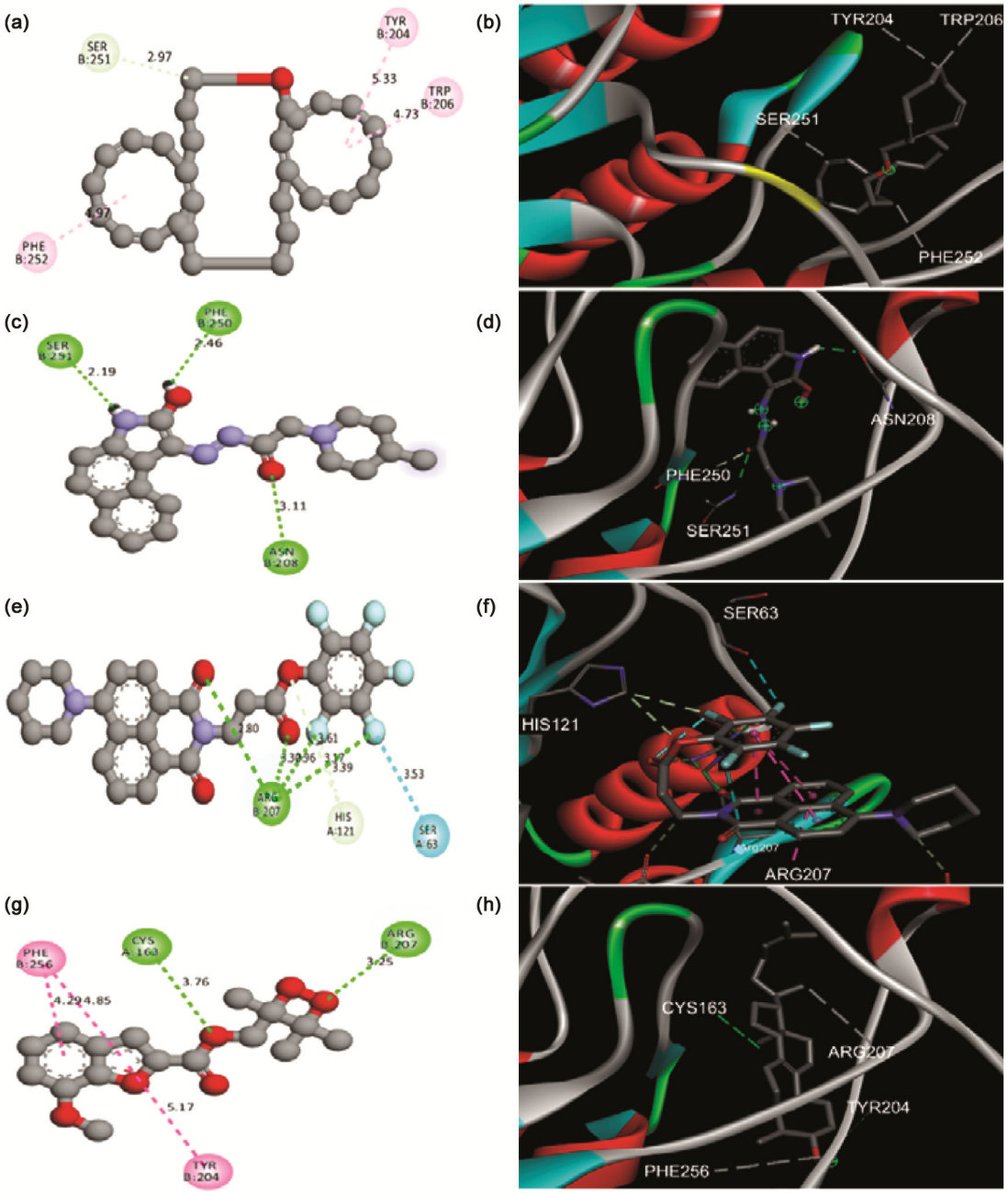

Fig. 5 — Graphical representation of molecular dynamics simulations showing Rg of ligand-protein complex over 100 ns period of simulations for four selected compounds.

end where it peaks at about 3.0 nm, indicating quite a bit of flexibility. On the other hand, compound CID-22212496 showed low fluctuations below 0.5 nm during the simulation process, indicating a very stable interaction with caspase-3 as shown in Fig. 6b.

Radius of Gyration (Rg) analysis

The obtained radius of gyration (Rg) analysis indicates how compact the caspase-3 protein remains upon binding with four different ligands during simulation (Fig. 6c). The structural changes of Rg for compound CID-5368332 are quite stable around 1.4 nm in the first half of the simulation and become more fluctuating around 1.5 nm at the close time of 80 nanoseconds, indicating the protein structure remains compact. Compound CID-135592970 also showed a bit of stability, with Rg values hovering between 1.4 and 1.45 nm, indicating that interaction is strong but a bit less consistent. For compound CID-6426095, the Rg fluctuates more openly between 1.4 and 1.6 nm. This continuous deviation of compactness shows that the protein undergoes many conformation changes, indicating less effectiveness at maintaining a stable protein-ligand complex. In contrast, compound CID-22212496 has a much more stable Rg pattern, with minimal fluctuations between 1.35 and 1.4 nm.

Table 6 — The pharmacokinetic and cytotoxicity predictions of the active constituents of *C. ternatea*

Compounds	MW	HBD	HBA	Log P	Log S	BBB Permeability	GI Absorption	Cytotoxicity
1CT	406.64	0	1	8.71	–9.88	No	Low	No
2CT	350.41	2	5	4.13	–5.67	No	High	No
3CT	518.43	0	9	6.73	–8.88	No	High	No
4CT	398.66	1	1	6.75	–7.93	No	Low	No

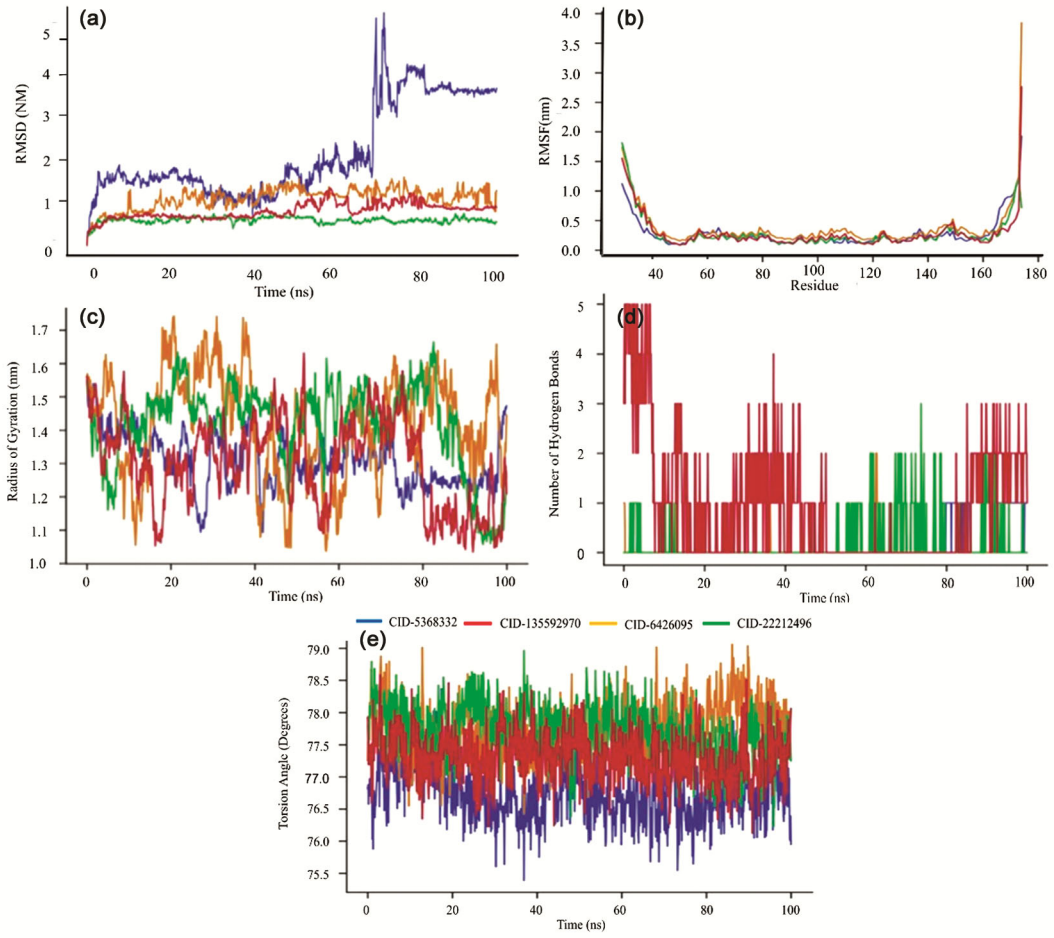

Fig. 6 — Graphical representation of molecular dynamics simulations showing SASA of ligand-protein complex over 100 ns period of simulations for four selected compounds.

Solvent Accessible Surface Area (SASA)

The Solvent Accessible Surface Area (SASA) represents an area of interest because it indicates potential structural rearrangements or fluctuations in the protein (Fig. 6d). In general, a stable SASA usually indicates that the protein retains its conformation on the surface, while larger fluctuations might indicate unfolding or expansion. In compound CID-5368332, a highly fluctuating SASA was observed. Also, compound CID-135592970 showed relatively stable values for SASA, with minor fluctuations, indicating that the compound supports the protein's structural integrity. For compound CID-6426095, there is a fluctuation pattern in SASA, again oscillating between higher and lower values to show a much less stable interaction. In contrast, the SASA profile of compound CID-22212496 showed more stability with fewer fluctuations during simulation process.

Ligand torsion profile (LTP) analysis

Ligand torsion profile (LTP) shows how the torsional flexibility changes for each compound throughout the simulation (Fig. 6e). It describes the rotation around a bond between any two atoms of the ligand. Overall, the smaller the deviations in torsional angles, the more rigid and stable the conformation of the ligand; the larger the deviation, the more flexibility within the ligand, which might determine the binding interaction. Compound CID-5368332 showed a moderate fluctuation; the angle fluctuates between 75.5 and 78º, indicating some flexibility in the conformation within caspase-3, but it could also indicate that the compound is not locking into a stable conformation. The regular oscillations indicate that the compound CID-5368332 does not have any solid binding mode and perhaps changes its torsion angles quite often to provide for the protein movements.

Compound CID-135592970 also showed relatively stable torsion angles with fluctuations ranging from 76 to 77.5 degrees, indicating a moderate level of flexibility compared to compounds CID- 5368332 and CID-6426095. For compound CID-6426095, more pronounced torsion angle fluctuations ranging between 75 and 79 degrees exist. In contrast, compound CID-22212496 has much smaller torsion angle fluctuations with values ranging between 76 and 77 degrees.

Ligand-protein energy interaction analysis

The interaction energies between caspase-3 and the four different compounds over the course of the simulation were evaluated. The graphs show two types of energy interactions: Coulomb short-range (Coul-SR) and Lennard-Jones short-range (LJ-SR), which help us to understand how the compounds interact with the protein at a molecular level. Coulomb interactions are electrostatic, while Lennard-Jones forces reflect van der Waals interactions, indicating how the compounds are stabilizing or destabilizing the protein complex.

In Fig. 7a, in compound CID-5368332, the Coul-SR energy (blue line) remains relatively stable throughout the simulation, hovering around –25 kJ/mol, indicating that the electrostatic interactions between the compound and the protein are stable with only minor fluctuations. The LJ-SR energy (orange line) starts near –50 kJ/mol and becomes more negative, stabilizing around –100 kJ/mol after approximately 50 nanoseconds, indicating involvement in strong non-covalent interactions contributing to the binding affinity. In Fig. 7b, compound CID-135592970 showed some degree of instability in both Coul-SR energy (blue line) and LJ-SR energy (orange line) interaction energies varying between –25 and –75 kJ/mol and around –75 to –100 kJ/mol, respectively, indicating that the interactions are not consistently stable with caspase-3 but become more stable by the end of the simulation.

In Fig. 7c, the interaction energies for compound CID-6426095 showed more instability. The Coul-SR energy (blue line) fluctuates heavily at the beginning of the simulation and then stabilizes between –25 and 0 kJ/mol after about 50 nanoseconds, indicating weak electrostatic interactions that may affect the stability of the ligand-protein complex. The LJ-SR energy (orange line) similarly fluctuates at the start with occasional drops to around –100 kJ/mol, but it remains close to zero for much of the simulation, indicating a weaker interaction with caspase-3. In Fig. 7d, compound CID-22212496 demonstrated highly stable interaction energies. The Coul-SR energy (blue line) remains consistently around –25 kJ/mol throughout the simulation, indicating strong and stable electrostatic interactions. The LJ-SR energy (orange line) remains steady around –100 kJ/mol, reflecting stable van der Waals interactions, indicating that the compound is tightly bound to caspase-3, forming strong and stable interactions with the protein.

Principal Component Analysis (PCA)

The Principal Component Analysis (PCA) plots for the trajectories of caspase-3 bound to the selected compounds during the MD simulation were evaluated.

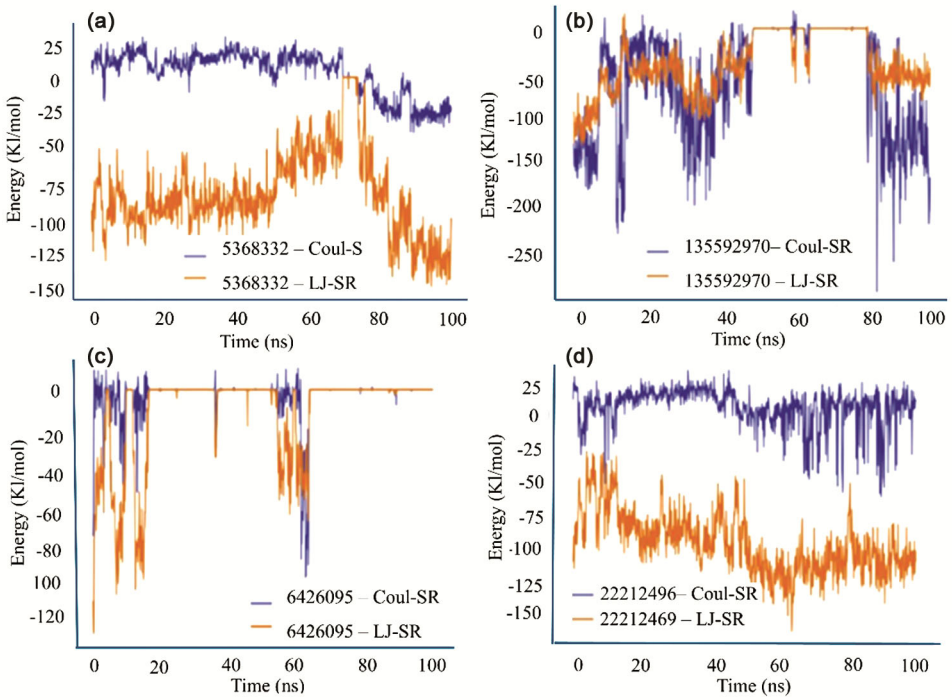

Fig. 7 — Graphical representation of molecular dynamics simulations showing LTP of ligand-protein complex over 100 ns period of simulations for four selected compounds.

PCA is used to analyze the motions of the protein by reducing the complexity of the data into principal components (eigenvectors) that represent the dominant motions. The tighter the clustering of points, the more confined and stable the motion, while broader distributions indicate more flexibility and variation in motion.

In Fig. 8a, the PCA plot for compound CID-5368332 showed two distinct clusters of points. The first cluster is centered around the origin while the second is displaced further along the x-axis. The spread of points within each cluster is relatively tight, indicating some degree of localized stability in the protein's motion. In Fig. 8b also, compound CID-135592970 showed two clusters. The clusters are moderately tight with points spread across a limited range of the x and y axes. The intermediate clustering indicates that the compound provides reasonable stability while still allowing the protein to explore multiple conformations.

For Fig. 8c, which represents compound CID-6426095, showed a much broader and more scattered distribution of points across both the x and y axes compared to other compounds. The points are spread widely, indicating that the protein-ligand complex is highly flexible with the protein exploring a wide range of conformations throughout the simulation. In Fig. 8d, the PCA plot for compound CID-22212496 showed two distinct clusters, but the points within each cluster are more tightly packed compared to compound CID-5368332.

Secondary Structure Element (SSE) compositions analysis

The secondary structure elementary (SSE) changes of caspase-3 bound to the four different compounds over the course of a 100-nanosecond molecular dynamics simulation were calculated. Using the provided color code, we can interpret the various structural elements in the protein, such as extended strands (E) bends (B) turns (T) alpha helices (H) and coils (C). Structural changes upon ligand binding can indicate how the protein's conformation adapts or stabilizes when interacting with a ligand.

In Fig. 9a, which represents the secondary structure changes of caspase-3 bound to compound CID-5368332, we observed that the overall structure remains relatively stable throughout the simulation. The yellow (extended strand) and pink (alpha helices) regions are consistent across most of the protein residues, indicating that the core secondary structures are largely preserved. There are some noticeable changes in the coil (green) and turn (cyan) regions, particularly towards the beginning and end of the

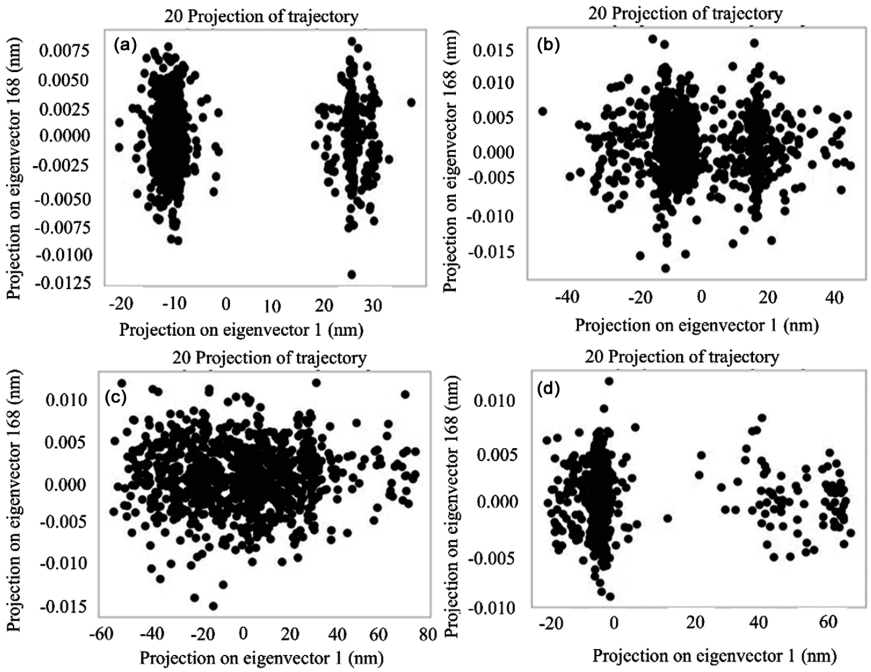

Fig. 8 — Interaction Energies plots showing Coul-SR and LJ-SR interactions for compounds: (a) CID-5368332, (b) CID-135592970, (c) CID-6426095, (d) CID-22212496 with caspase-3.

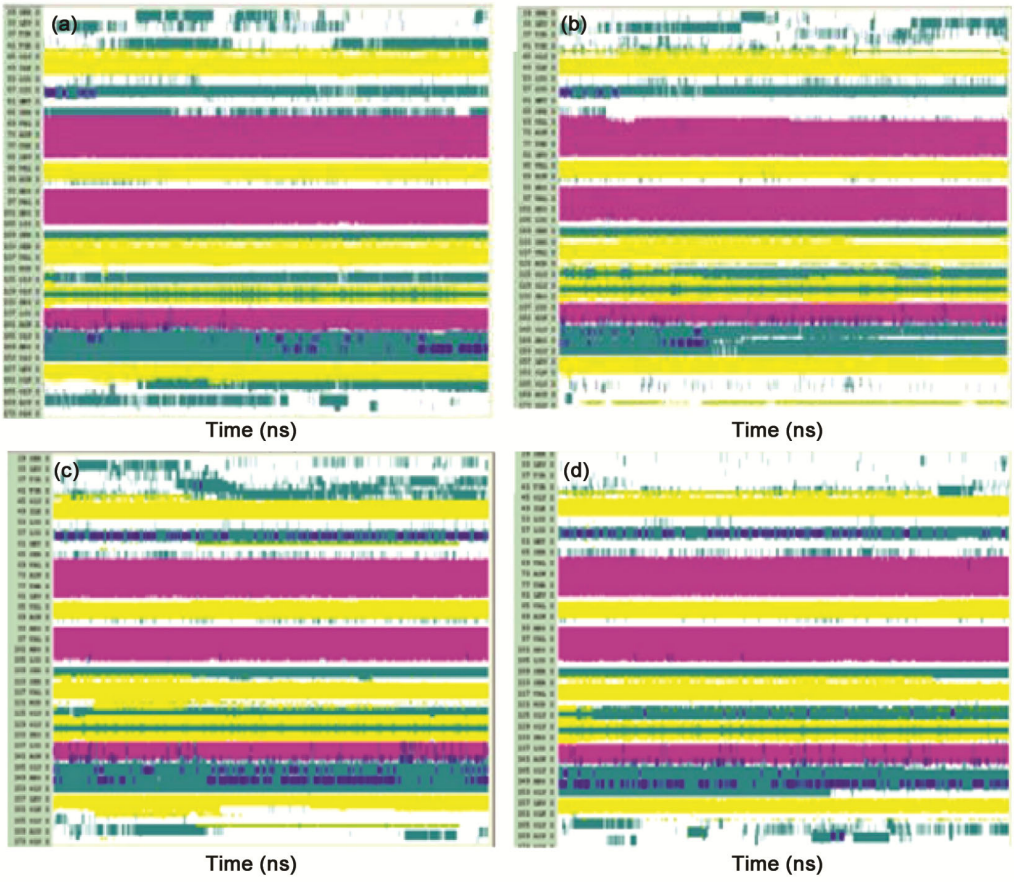

Fig. 9 — PCA ligand-protein complex of compounds: (a) CID-5368332, (B) CID-135592970, (C) CID-22212496, (D) CID-135592970 with caspase-3.

sequence, indicating some flexibility in the loop regions, but the more structured elements like helices and beta strands remain stable. In Fig. 9b, which represents compound CID-135592970, there is some moderate fluctuation in the secondary structure, although not as pronounced as with compound CID-6426095. The pink and yellow regions remain largely intact, indicating that the helices and beta strands are stable, but there are more regions where coils (green) and turns (cyan) appear, indicating that while the core structure remains intact, the protein exhibits some flexibility in its loop and turn regions.

In Fig. 9c, which corresponds to compound CID-6426095, there is significantly more variation in the secondary structure over the course of the simulation. The pink alpha helices and yellow beta strands are disrupted at several points with more frequent shifts into green coils and cyan turns, indicating it induces more conformational changes in the protein, particularly in regions that were previously more structured. In Fig. 9d, which represents compound CID-22212496, the extended strands (yellow) and alpha helices (pink) remain consistent across most of the protein with only minor fluctuations in the coil and turn regions (green and cyan).

Amino acid interaction and decomposition energy analysis

The decomposition energy plots display the interaction energy between specific amino acid residues of caspase-3 and the four different ligands over the course of the simulation. These interactions broken down by individual residues reveal which parts of the protein are contributing most to the binding energy with each ligand. The color gradient from red to blue indicates the strength of these interactions, with more negative (blue/purple) values representing stronger binding interactions.

In Fig. 10a, which showed the decomposition energy plot for compound CID-5368332, the interaction energy is concentrated around several key residues, particularly ARG-14, SER-10, and LYS-14. The dark blue regions indicate strong binding interactions between these residues and the compound with energy values around –200 to –250 kcal/mol. The uniformity of these strong interactions across the

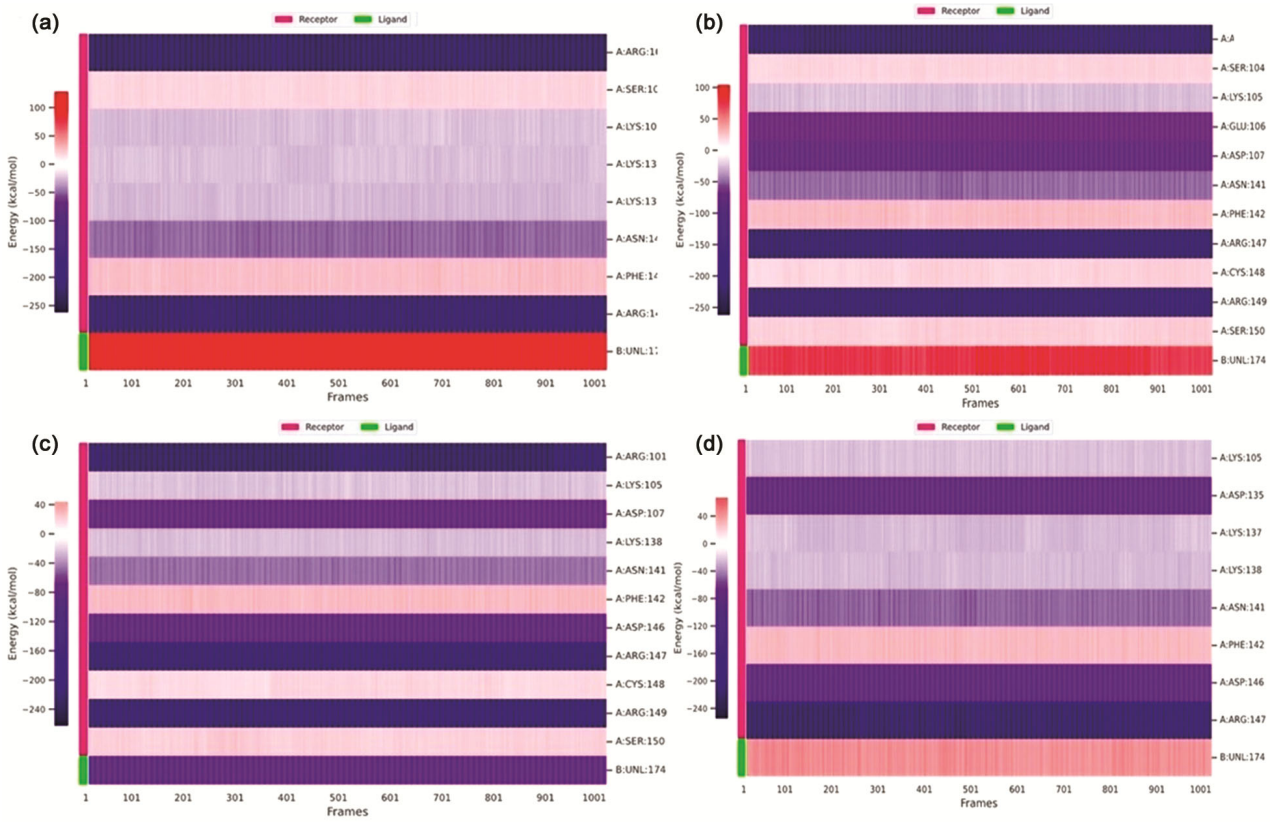

Fig. 10 — SSE composition analysis ligand-protein complex for compounds:(a) CID-5368332, (b) CID-135592970, (c) CID-6426095, (d) CID-22212496 with caspase-3.

simulation frames indicates stable and consistent binding. There are some lighter regions, particularly with ASN-14 and PHE-14, where the interaction energy is weaker, suggesting that not all residues contribute equally to the binding stability. In Fig. 10b, compound CID-135592970 showed a moderate interaction energy pattern. The key residues, such as ARG-101, GLU-106, and ASP-107, demonstrate strong binding with energies around –150 to –200 kcal/mol. In some regions, particularly around SER-150 and CYS-148, weaker interactions were shown, which may indicate some instability in the compound's binding. This may allow for some flexibility in the binding pocket, but overall, it maintains a reasonably stable interaction with the protein.

In Fig. 10c, the decomposition energy plot for compound CID-6426095 shows a slightly different pattern. The interactions here are more spread out, with key residues of ARG-101, LYS-105, and ASP-107 displaying strong binding energies (around –150 to –200 kcal/mol). The plot also showed several regions where the interaction energy is weaker or even positive, such as with CYS-148 and SER-150. This variability indicates that the compound does not bind as consistently or strongly to all residues. The variation in energy across the frames and the different residues suggests that ligand may not form as stable an interaction with caspase-3 as compound CID-5368332. The weaker interactions with certain residues may contribute to the instability shown in the RMSD and secondary structure plots. Fig. 10d, which represents compound CID-22212496, showed a much more stable and consistent binding profile. The strong blue regions around residues LYS-105, ASP-135, and ASN-141 indicate very strong interactions with binding energies consistently around –200 to –250 kcal/mol throughout the simulation.

Free energy analysis of ligand-protein complex

The bar plots in Fig. 11 represent the free energy components for the interaction between caspase-3 and the four selected compounds from *C. ternatea*. These include enthalpy (ΔH) entropy contribution (–TΔS), and the overall Gibbs energy (ΔG). Free energy components help us understand the thermodynamic favorability of binding. Lower ΔG values indicate more favorable spontaneous binding interactions, while the enthalpy and entropy components give insight into the driving forces behind the binding.

In Fig. 11a, which represents compound CID-5368332, the ΔH (enthalpy) is negative, around

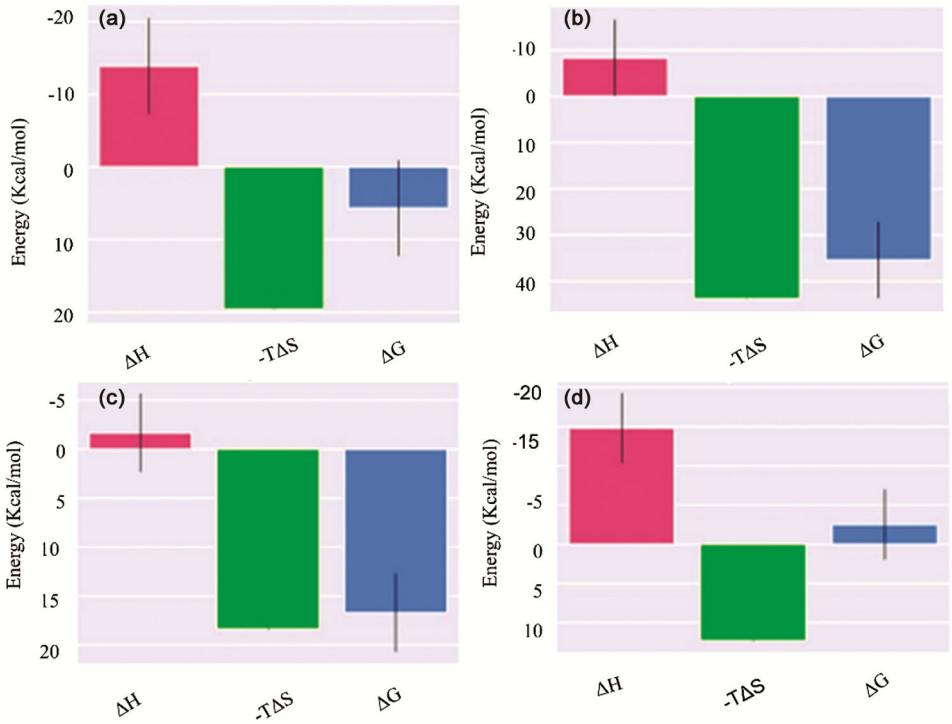

Fig. 11 — Decomposition energy plot of protein with compounds: (a) CID-5368332, (b) CID- 135592970, (c) CID-6426095, (d) CID-22212496 with caspase-3.

–15 kcal/mol, which indicates that the binding interaction is exothermic and energetically favorable from an enthalpic standpoint. The –TΔS (entropy contribution) is positive around 10 kcal/mol, indicating an unfavorable entropy contribution to the binding. This could be due to the restriction of conformational freedom in the ligand or protein upon binding. Despite the entropy loss, the overall ΔG is slightly negative, indicating that the binding interaction is still favorable but not very strong. The small magnitude of ΔG indicates that the compound binds to caspase-3 with modest affinity where the enthalpic contributions outweigh the entropic costs. In Fig. 11b, compound CID-135592970, the ΔH is only slightly negative around –10 kcal/mol indicating week enthalpic binding contributions. The –TΔS component is positive and large, around 25 kcal/mol, indicating a significant entropic cost upon binding. This high entropy loss indicates a considerable reduction in flexibility or conformational freedom during the binding process. The overall ΔG is positive, indicating that the binding interaction is thermodynamically unfavorable, which may not form a strong or spontaneous interaction with caspase-3.

In Fig. 11c, compound CID-6426095, the ΔH is close to zero, suggesting that the binding interaction is neither strongly exothermic nor endothermic. The –TΔS component is significantly positive around 15 kcal/mol, indicating a large unfavorable entropy contribution. This high entropy loss indicates that the compound or protein loses a considerable amount of conformational freedom upon binding. The overall ΔG is positive, indicating that the binding interaction is thermodynamically unfavorable and may not form a spontaneous or strong interaction with the protein. In Fig. 11d, compound CID-22212496, the ΔH is strongly negative around –18 kcal/mol, indicating that the binding is highly exothermic and enthalpically favorable. The –TΔS component is positive around 7 kcal/mol, but it is much smaller than in the previous ligands, indicating that there is less entropic cost associated with the binding. The overall ΔG is slightly negative, indicating that the binding interaction is favorable and spontaneous. The strong enthalpic contribution combined with a relatively small entropy penalty suggests that the compound forms a highly stable interaction with caspase-3.

Acute toxicity and cell death analysis

The antiproliferative MTT assay is the first indication to be evaluated when investigating novel anticancer agents. The normal cell line HSF treated with DOX exhibited a significant reduction in cell growth at various concentrations with a IC_{50}value of 1.135±2.35 µg/mL following 24 h (Fig. 12a), whereas the ethoxy extraction of *C. ternatea* showed no cytotoxic activities on the normal cell line HSF with a IC_{50}value of 869.6±5.04 µg/mL (Fig. 12b). The IC_{50} values of anticancer activity of ethoxy extract were presented in Table 7. However, in contrast to the BC cell line MDA-MB-231 treated with DOX (Fig. 13a) which showed a significant inhibition in cell viability,

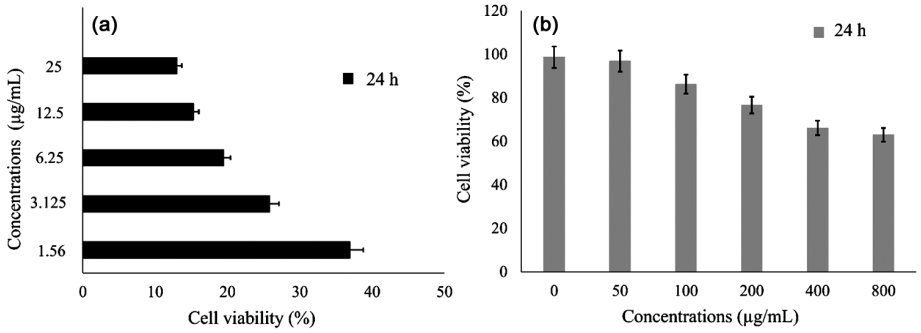

Fig. 12 — Gibbs free energy values of the ligand-protein complex for compounds: (a) CID-5368332, (b) CID-135592970 (c) CID-6426095, (d) CID-22212496 with caspase-3.

Table 7 — IC50 values of the normal HSF and BC cell lines treated with *C. ternatea* for 24 h and 48 h

		Experimental cell lines			
		HSF	MCF-7	T47D	MDA-MB-231
Treatments	24 h	1.135±2.35			1.27±0.12
DOX	24 h	869.6±5.04	397.7±4.60	433.8±5.73	363.6±6.94
C. terantea	48 h		222.03±3.25	239.07±2.73	209.4±4.06

all the BC cell lines treated with *C. ternatea* extract showed no inhibition in cell proliferation at concentrations of 50, 100, and 200 µg/mL, whereas higher concentrations of 400 µg/mL and 800 µg/mL showed significant reductions in cell viability percentages, particularly in the BC cell line MDA-MB-231 (Fig. 13d), followed by the BC cell lines MCF-7 (Fig. 13b) and T47D (Fig. 13c) following 24 h and 48 h, respectively. In scientific research, when using medicinal plants or isolated compounds, the SI value should be considered. In this study, we calculated the SI values for all experimental studied BC cell lines by dividing the IC_{50}value of the normal cell line HSF by the IC_{50} value of each BC cell lines MCF-7, T47D, and MDA-MB-231. We found that SI values (SI > 2), following 24 h and 48 h, as presented in Table 8.

Microscopical analysis

The morphological changes of studied normal fibroblasts and BC cell lines were examined using phase-contrast microscopy. The microscopical examinations showed that the normal cell line HSF maintains its spindle shape with intact cell membranes and nuclei, indicating no cytotoxic effects of isolated components (Fig. 14). In comparison to untreated cancer cells (control), which displayed a phenotypic resemblance to fibroblasts and were incredibly confluent, the treated BC cell lines MCF-7 (Fig. 15), T47D (Fig. 16), and MDA-MB-231 (Fig. 17) with *C. ternatea* extract at a concentration of 50, 100, and 200 µg/mL showed minimal morphological changes, and most of the cells still retained their tumorigenic characteristics. Meanwhile, cancer cells treated at a concentration of 400 µg/mL began to lose their spindle shape and experience several cellular deformations, such as the formation of apoptotic bodies. Moreover, the morphological changes become more apparent at a higher concentration of 800 µl/mL, where there is a notable reduction in the number of viable cells and increasing detaching cells, suggesting that cancer cells are being induced to death.

Caspase-3 activation analysis

An increase in the activity of caspase-3 was determined. CASPASE-Glo luminometric analysis of these proteins revealed a highly significant increase (< 0.001) in the level of the enzymes in the treated BC cell line MDA-MB-231 (of interest) with *C. ternatea* compared to treated with DOX (Fig. 18).

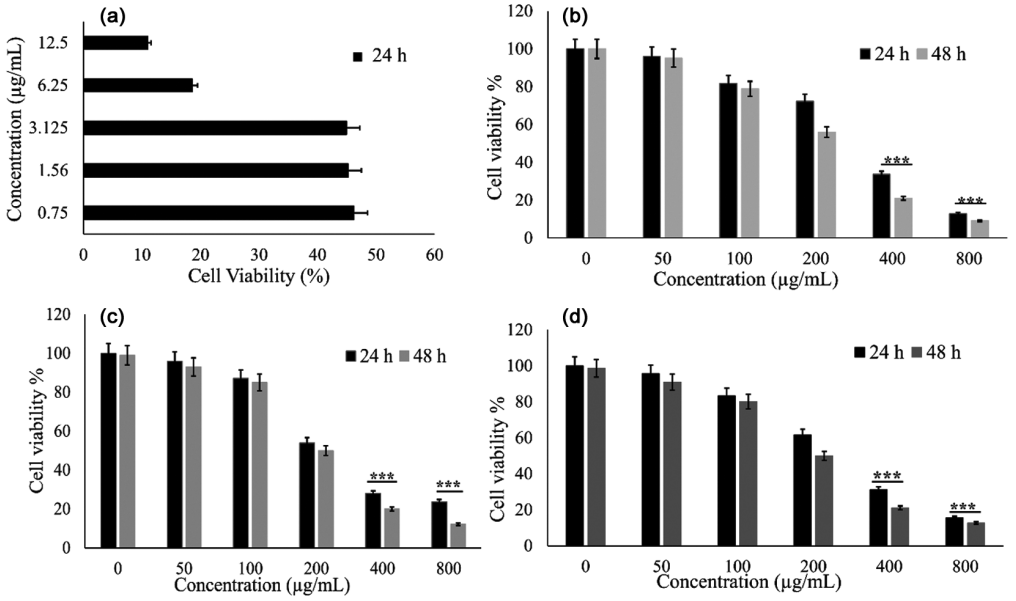

Fig.13 — Cell viability of normal HSFs cells treated with: (a) Pure ethanolic C. ternatea extract, and (b) DOX for 24 h of treatment.

Table 8 — SI values of ethoxy extraction of *C. ternatea*

		Experimental cell lines			Recommendation range [1.96 – 51.3][28]
		MCF-7	T47D	MDA-MB-231	
SI values	24 h	2.19	2.00	2.39	
	48 h	3.91	3.64	4.15	

Discussion

Understanding molecular docking, dynamic simulation, and computational pharmacokinetics of bioactive compounds of plant origin is becoming a considerable attention in the discovery of novel drug candidates because of their low cost and toxicity. Finding alternative therapeutic choices instead of chemoradiotherapies targeting metastatic BC cells with fewer toxic effects on the normal healthy cells was our main objective. In this study, we evaluated the acute toxicity and anticancer activity of phytochemical constituents of *C. ternatea* flowers on the normal cell line HSF and different BC cell lines by employing molecular caspase-3 modeling. To identify the main bioactive compounds, blue tea flowers were macerated in ethanol due to its advantage over other commercial solvents. Furthermore, the ethyl group in ethanol may draw non-polar phytoconstituents such as phenolics, flavonoids, fatty acids, and alcohol hydrocarbons. Ethanol is considered a safe, non-toxic polar solvent[32]. Since the solvent evaporation method had a significant impact on the composition of phenolic-aromatic compounds, a precision economy incubator was used to lower the boiling point of the ethanol and preserve the volatile constituents of the extract.

The UV-VIS and FTIR spectra analysis indicated the presence of specific functional groups[33] that

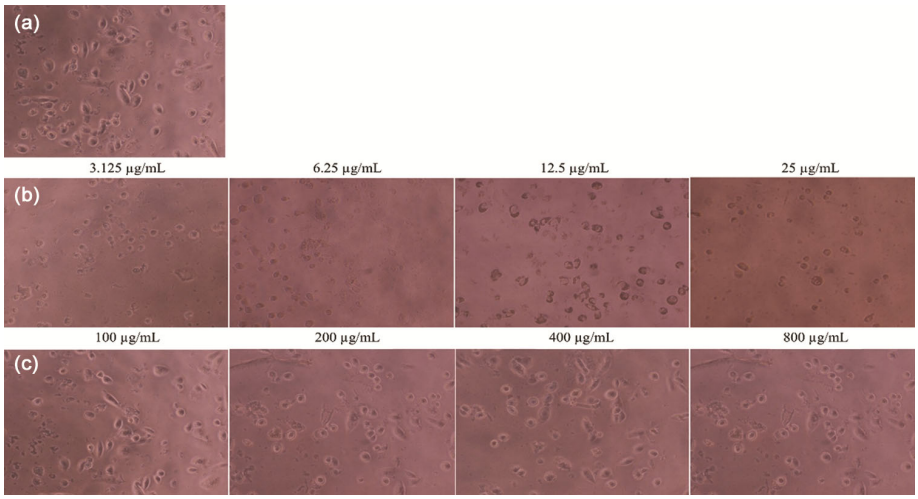

Fig. 14 — MTT assay showing cell viability percentages of different breast: (a) MCF-7, (b) T47D, (c) MDA-MB-231 cancer cells treated with C. ternatea, in comparison to (d) Breast MDA-MB-231 cancer cells treated with DOX at different concentrations. P-values < 0.05 was considered significant. P-value<0.001 was represented by *** asterisk.

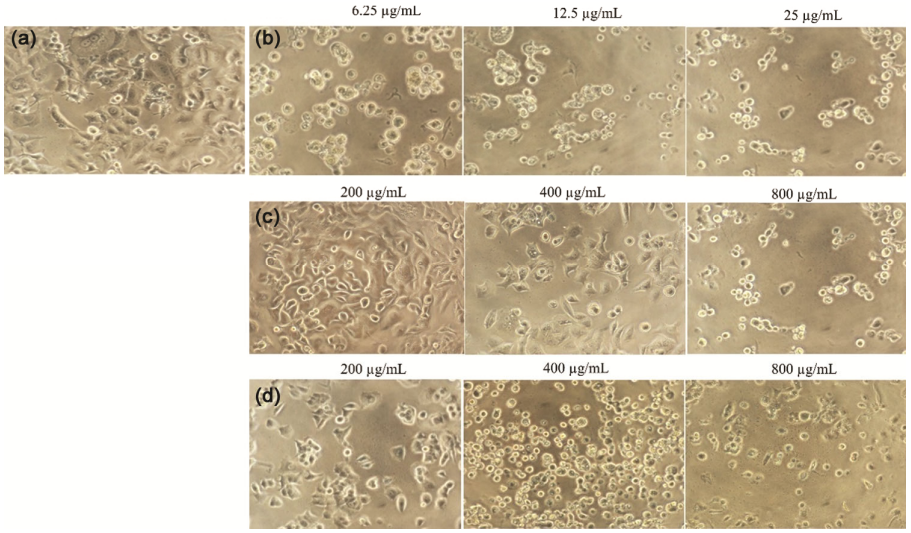

Fig. 15 — Morphological changes of normal HSFs treated with DOX, and C. ternatea (CT) extract at various concentrations for 24 hours, compared to untreated cells (Control). Images were taken at 20x magnification.

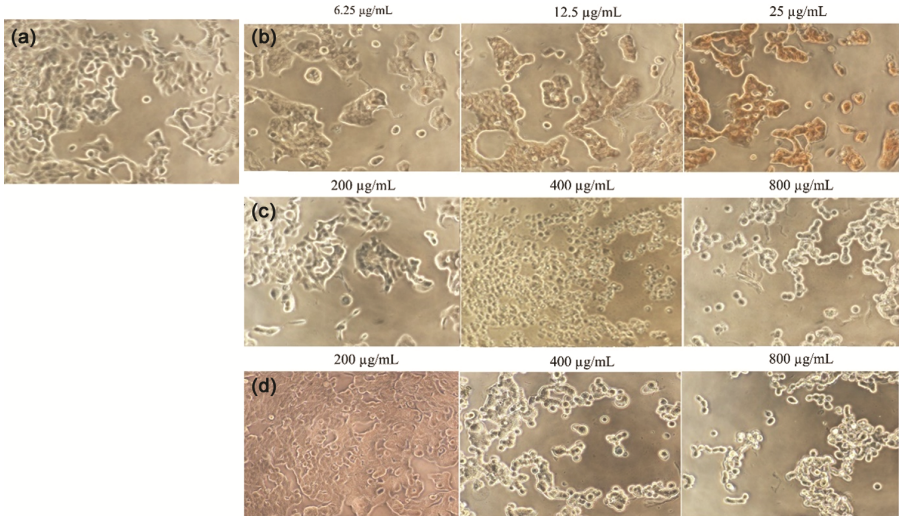

Fig. 16 — Morphological changes of breast MCF-7 cancer cells treated with DOX at different concentrations (3.125, 6.25, and 12.5 µg/ml) for 24 hours, and C. ternatea (CT) extract at different concentrations (200, 400, and 800 µg/ml) for 24 and 48 hours, compared to untreated cells (Control). Images were taken at 20x magnification.

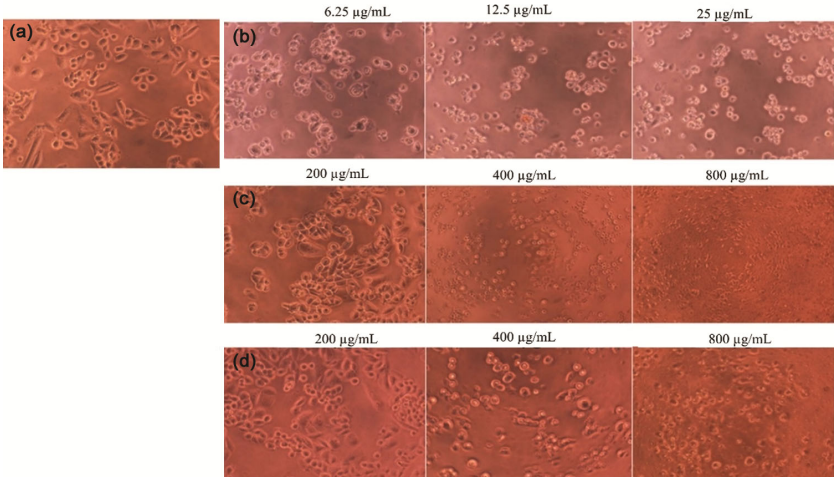

Fig. 17 — Morphological changes of breast T47D cancer cells treated with DOX at different concentrations (3.125, 6.25, and 12.5 µg/ml) for 24 hours, and C. ternatea (CT) extract at different concentrations (200, 400, and 800 µg/ml) for 24 and 48 hours, compared to untreated cells (Control). Images were taken at 20x magnification.

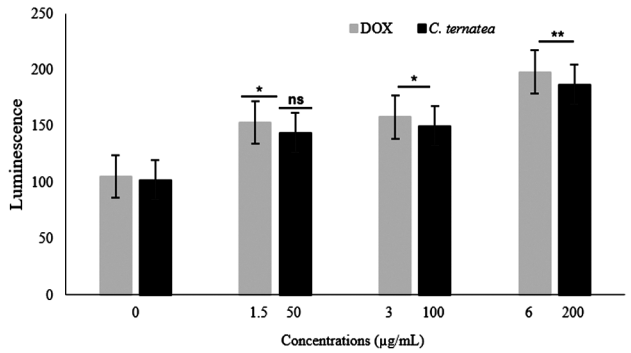

Fig. 18 — Morphological changes of breast MDA-MB-231 cancer cells treated with DOX for 24 hours, and C. ternatea extract at various concentrations for 24 and 48 hours, compared to untreated cells (Control). Images were taken at 20x magnification.

revealed high intensity of phenolics, aromatic, and amin components, different from reported previous studies[34,35]. Gas chromatography spectra showed different major compounds with different peak intensities. Our findings are in line with previous studies that reported significant promising effectiveness of phenolics as cytotoxic anticancer drugs that inhibit proliferation and progression of cancer cells through targeting oncogenic signaling pathways[36,37].

However, from a total of 13 isolated compounds, four interesting components were identified in the ethoxy extract of *C. ternatea* using gas chromatography. Pyrazoline/ imidazole ($C_3H_4N_2$), a class of heterocyclic compounds, has shown essential biological activities as

anti-inflammatory and anticancer candidates[38]. Piperidine, another heterocyclic compound $(CH_2)_5NH$, is a promising component showing anticancer activities when used alone as well as conjugated with other drug candidates against different malignancies, through arresting the cell cycle and inhibiting cancer cell viability[39]. Isoquinolin (C_9H_7N) compound, demonstrate a variety of biological actions, against various microorganisms and cancer cells, as well as to reverse multidrug resistance[40]. A similar compound: 3-oxatricyclo-triaconta-hexaene ($C_{29}H_{42}O$) to our isolated compound (of interest) cholesta-8,24-dien-3-ol ($C_{27}H_{44}O$), showed antioxidant activity against the BC cell line MCF-7[41].

Computer-drug design can forecast the compounds' efficacy and cut down on the time and expense required to identify new treatments[42], by enabling focused, quick, and simple research, bioinformatic validatory algorithms, and molecular simulation of newly discovering compounds. Primarily at the nanoscale level, the field of nano-bioinformatics is a response to the growing demand for novel medications and focused drug therapy[43]. The isolated bioactive compounds from *C. ternatea* showed higher binding affinity with caspase-3; this can be explained by the formation of many hydrogen bonds, hydrophobic interactions, and halogen bonds. Patil *et al.*[44] found that both hydrogen and hydrophobic bonds are playing a vital role in stabilizing the ligands at the active target sites and can alter binding affinity and drug efficacy. Also, Xu *et al.*[45] have reported that halogen bonds are key players in improving drug-target binding affinity.

Additionally, the MW of bioactive compounds can correlate well with solubility, cellular membrane permeability, and passive diffusion, since low MW compounds are probably highly absorbed, diffused, and transported across membranes[46]. Recently, one big obstacle facing researchers and scientists is ineffective medications from natural sources against targeted organisms. Computational pharmacokinetic predictions showed that about 50% of isolated compounds from *C. ternatea* have poor solubility, which may affect their efficiency when targeting the BC cells. Consequently, low bioavailability can result from low solubility and permeability of molecules[47].

Recent studies[48-50] revealed that the *C. ternatea* flower extract's biomolecular active compounds have the potential to target different apoptotic signaling pathways. In this study, we intend to investigate a different direction of inducing the intrinsic apoptotic pathway *via* activation of caspae-3 protein. The stability property in RMSD is often correlated with strong binding affinity, which is crucial for the effectiveness of potential drugs. Stable binding affinity is typically indicated by lower RMSD values[51]. The significance of RMSF analysis in comprehending protein-ligand interactions has been emphasized by recent research. Drug design is impacted by these interactions and how RMSF data can forecast the functional effects of ligand binding on protein dynamics is covered by Townsend *et al.*[51]; they stress that good simulation data interpretation requires precise tools. Compared to the other isolated compounds, MD simulation of RMSD and RMSF exhibited lower interaction values in the compound (of interest) CID-22212496. Also, the stability of Rg patterns in compound CID-22212496 was observed through the simulation, indicating that the protein is in a rigid state. These findings were correlated with the SASA profile that revealed much more stability, which is highly desirable from a drug discovery perspective. Additionally, lower deviations in LTP values may indicate maintaining a more rigid conformation in this compound throughout the simulation process.

Moreover, the Coul-SR and LJ-SR energies maintain stable van der Waals interactions with the caspase-3 protein, indicating strong electrostatic interactions compared to other compounds. The tight clustering of points in the PCA plot indicates that the protein-ligand complex remains stable within each conformational state, suggesting strong binding and stable dynamics for compound CID-22212496. The SSE compositions of this compound remain remarkably stable and the strong blue regions around certain amino acid residues, such as LYS-105, ASP-135, and ASN-141, indicate stable and continuous interactions across all frames, suggesting that compound CID-22212496 forms a very strong and stable interaction with caspase-3. This aligns with the earlier analyses where compound CID-22212496 consistently showed the most stable and favorable interactions. Similar studies revealed significant effects of biomolecular compounds of *C. ternatea* docked with high binding affinity and rigidity[52,51].

Evaluating extracted herbal compounds for anti-cancer medications, either using cancer cell lines *in vitro* or *in vivo* models without determining SI, is a poor predictor for upcoming experiments[53]. Herein, we found that the isolated compounds from *C. terantea* display non-toxic activity on the normal cell line HSF. These results are correlated with Jeyaraj *et al.*[6], who found that active compounds of *C. ternatea* exhibited no toxic effects on the normal human foreskin fibroblast cell line

(Hs27). However, ideal isolated compounds can affect the cancer cells without impacting the normal cells. The bioactivity of several medicinal plants has been documented in innumerable scholarly publications without including SI data. Our findings are in line with Famuyide *et al.*[54], who proposed that SI values < 1, indicate toxic compounds and not suitable for use as medication.

In this study, the ethoxy *C. ternatea* flower extract exhibited the most potent cytotoxic activity against the metastatic TNBC cell line MDA-MB-231, followed by the positive estrogen-receptor breast adenocarcinoma cell line (MCF-7) and ductal adenocarcinoma (T47D), respectively. This could be attributed to the effects of phenolic aromatic organic compounds, which may exhibit aromatase inhibition activities that intermittently inhibit the enzyme activity of aromatase in estrogen biosynthesis, resulting in the blocking of androgen receptor[55]. Our findings are in line with Salleh *et al.*[56] and Asysyifa *et al.*,[57] who found that various solvent extractions of blue *C. ternatea* flowers showed a dose-dependent effect at higher concentrations. On the other hand, a recent study by Geethanjali *et al.*,[58] who found that roots of *C. ternatea* showed no significant cytotoxicity against the BC cell line MCF-7. We suggest that the hydrophobicity of phytochemical compounds of *C. ternatea* and the heterogenicity of cancer cells may impact their response to treatment.

Different subtypes of BC cells are genetically and clinically diverse in hormonal expression and prognostic factors. The expression of the hormone receptors (ER, PR, and HER2) is the basis for the most popular and generally recognized classification of BC cells[59]. However, in cancer research, targeting hormonal receptors of BC cells through a better understanding of the drug compositions and how its binding impacts the dynamics of the target protein may open new directions to develop anticancer medications. According to Atanasov *et al.*[60], green natural substances have proven to be a valuable and plentiful source of remedies for a variety of human ailments, including cancer. Several biochemical processes that trigger apoptosis and slow the progression of cancer cells are part of the anticancer cancer process, and because of its importance and complexity in tumor regression, apoptosis is one of the most important topics that is extensively researched in cancer research[61]. Caspases are essential for apoptosis promotion and the establishment of cellular morphology involved in programmed cell death[62]. Accordingly, a poor prognosis and the expression of apoptosis-associated proteins are tightly linked to caspase-3 in the BC cells[63]. Herein, a significant increase in activity of caspase-3 enzyme levels was observed in the metastatic TNBC cell line MDA-MB-231 (of interest) treated with IC_{50} doses of DOX and *C. ternatea* extract, which confirmed the earlier inhibition of cell proliferation, suggesting dose-dependent effects of *C. ternatea* at higher concentrations may induce cell cycle arrest through activation of the apoptotic caspase-3 pathway of the metastatic TNBC cell line MDA-MB-231. Overall, our comprehensive biomolecular investigations shed light on the isolation of major phytochemical organic components extracted from blue *C. ternatea* flowers as potential anticancer agents and how molecular dynamic interactions and hydrophobicity of extracted compounds may affect their bioactivities and stability when targeting cancer cells.

Conclusion

The presented results revealed novel phenyl amino benzoic acid compounds from *C. ternatea* flower with a high intensity of phenolics, aromatic, and amine components; using the tri-spectroscopy techniques, four compounds (1CT-4CT) were selected from a total of 13 compounds to evaluate their anticancer activity against different estrogen-receptor BC cell lines at the molecular level. Among these four compounds, compound 4CT: CID-22212496 (Cholesta-8,24-dien-3-ol) exhibited well-qualified stability, maintaining its rigid and optimal conformation with the least torsional flexibility throughout the simulation process. Moreover, these compounds showed no cytotoxic effects on the normal cell line HSF, whereas a higher significant reduction in cancer cell viability was observed at higher concentrated doses in the metastatic TNBC cell line MDA-MB-231 than in the BC cell lines MCF-7 and T47D. This could be attributed to the hydrophobicity of isolated ethoxy compounds and the heterogenicity of cancer cells that may impact their response to treatment. We suggest that isolated phenyl amino benzoic acid organic compounds may block estrogen receptors of cultured BC cells and subsequently inhibit estrogen synthesis.

Acknowledgment

The authors gratefully acknowledge technical and financial support provided by the Deanship of Scientific Research (DSR), King Abdulaziz University, Jeddah, Saudi Arabia, under grant no. (GPIP-480-130-2024).

References

1 Bray F, Laversanne M, Weiderpass E & Soerjomataram I, *Cancer*, 16 (2021) 3029.

2 Toungos M D, *Int J Innov Food Nut Sust Agri*, 6 (2019) 14.
3 Bergin A R T & Loi S, *F1000 Research*, 8 (2019) 1342.
4 Haroon F, Farwa U, Arif M, Raza M A, Sandhu Z A, El Oirdi M, Farhan M & Alhasawi M A I, *Biomed*, 11 (2023) 2686.
5 Ahad B, Shahri W, Rasool H, Reshi Z A, Rasool S & Hussain T, 1 (2021) 40.
6 Dave A, Parande F, Park E-J & Pezzuto J M, *J Can Met Treatment*, 6 (2020) 46.
7 Jeyaraj E J, Lim Y Y, Choo WS, *J Food Sci Tech*, 2054 (2021) 2067.
8 Purnamayanti A, Gondokesumo M E & Budipramana K, *Pharma Sci Rese* (PSR), 109 (2022) 124.
9 Mandal S M, Chakraborty D & Dey S, *Plant Signal Beh*, 359 (2010) 68.
10 Anantharaju P G, Gowda P C, Vimalambike M G & Madhunapantula S V, *Nutr J*, 15 (2016) 99.
11 Zhao B & Hu M, *Oncol Lett*, 1749 (2013) 1755.
12 Lin H H, Chen J H, Chou F P & Wang C J, *Br J Pharmacol*, 237 (2011) 54.
13 Feng S, Zha Z, Wang Z, Yang P, Wu J, Li X & Liu Y, *Nat Prod Rese*, 4865 (2021) 4869.
14 Kashyap D, Garg VK & Goel N, *Adv Protein Chem Struc Bio*, 73 (2021) 120.
15 Singh A, & Jain A K, *Indian J Agri Biochem*, 51 (2022) 57.
16 Carneiro B A & El-Deiry W S, *Nat Rev Clin Onc*, 395 (2020) 417.
17 Raval K & Ganatra T, *IP Inter J Comp Adv Pharm,* 12 (2022) 16.
18 Bennour, N, Mighri, H, Eljani, H, Zammouri T & Akrout A, *South African J Bota*, 181 (2020) 190.
19 Patel TK, Shrivas K, Kurrey R, Upadhyay S, Jangde R & Chauhan R, *Spectrochim Acta A Mol Biomol Spectrosc*, 242 (2020) 118717.
20 Shahmoradi R, Talebibahmanbigloo N, Javidparvar A, Bahlakeh G & Ramezanzadeh B, *J Mol Liq*, 304 (2020) 112751.
21 Pangesti P, Masruri M, *In IOP Conference Series: Materials Science and Engineering*, 833 (2020) 012033.
22 Hago S, Lu T, Alzain AA, Abdelgadir AA, Yassin S, Ahmed EM & Xu H, *Nat Prod Res*, 1073 (2023) 1079.
23 Yahaya MAF, Bakar ARA, Stanslas J, Nordin N, Zainol M & Mehat MZ, *BMC Biotech*, 21(2021) 38.
24 Vanommeslaeghe K & MacKerell AD Jr, *J Chem Inf Model*, 44 (2012) 54.
25 Best R B, Zhu X, Shim J, Lopes P E, Mittal J, Feig M & Mackerell J A, *J Chem Theory Comp*, 3257 (2012) 3273.
26 Abraham M J, Murtola T, Schulz R, Páll S, Smith J C, Hess, B & Lindahl E, *Software X*, 19 (2015) 25.
27 Kamiloglu S, Sari G, Ozdal T & Capanoglu E, *Food Frontiers*, 332 (2020) 349.
28 Indrayanto G, Putra G S & Suhud F, *Profiles Drug Sub Excip Rel Meth*, 46 (2021) 307.
29 Bhatia D & Malik D, *Advan AI Tech Applic Bioinfo*, 17 (2010) 40.
30 Patil R, Das S, Stanley A, Yadav L, Sudhakar A & Varma AK, *PLoS One*, 5 (2010) e12029.
31 Xu Z, Yang Z, Liu Y, Lu Y, Chen K & Zhu W, *J Chem Inf Model*, 69 (2014) 78.
32 Abubakar AR & Haque M, *J Pharm Bioallied Sci*, 1 (2020) 10.
33 Hong T, Yin J Y, Nie S P & Xie M Y, *Food Chem X*, 12 (2021) 100168.
34 Singh A & Jain K, *Indian J Agri Biochem*, 51 (2022) 57.
35 Yolin Angel PASR, Jeyakumar P, Jasmin Suriya AR, Sheena A, Karuppiah P, Periyasami G, Stalin A & Murugan K, *Front Microbiol*, 15 (2024) 1343988.
36 Rahaiee S, Assadpour E, Faridi Esfanjani A, Silva A S & Jafari S M, *Adv Colloid Interface Sci*, 279 (2020) 102153.
37 Choudhari A S, Mandave P C, Deshpande M, Ranjekar P & Prakash O, *Front Pharmacol*, 10 (2020) 1614.
38 Alahmdi M I, Khasim S, Vanaraj S, Panneerselvam C, Mahmoud M M A, Mukhtar S & Aldosari O F, 2022, *J Inorg Organomet Poly Mat*, 2146 (2022) 2159.
39 Mitra S, Anand U, Jha N K, Shekhawat M S, Saha S C, Nongdam P, Rengasamy KRR, Proćków J & Dey A, *Front Pharmacol*, 12 (2021) 772418.
40 Maza L J G, Salgado A M, Kouznetsov V V & Meléndez C M, *RSC Adv*, 1710 (2024) 1728.
41 Qurishi Y, Seshadri D, Poyil M, Franklin B, Apte A, Alsharif K & Zaki M, *J King Saud Uni-Sci*, 33 (2021) 101418.
42 Sliwoski G, Kothiwale S, Meiler J & Lowe EW, *Pharm Rev*, 334 (2013) 95.
43 Bhatia D & Malik D, *Advan AI Tech Applic Bioinfo*, 17 (2010) 40.
44 Patil R, Das S, Stanley A, Yadav L, Sudhakar A & Varma AK, *PLoS One*, 5 (2010) e12029.
45 Xu Z, Yang Z, Liu Y, Lu Y, Chen K & Zhu W, *J Chem Inf Model*, 69 (2014) 78.
46 Savjani K T, Gajjar A K, & Savjani J K, *Intern Schol Rese Notices*, 1 (2012) 195727.
47 Shukla R, & Tripathi T, *Computer-aided drug design*, 133 (2020)161.
48 Rollando R, Amelia A, Afthoni H & Prilianti R, *J. Pure Appl. Chem. Res*, 7 (2023) 14.
49 Muna I, Amalina D & Husain A, *Int J Cell Biomed Sci*, 2 (2023) 142.
50 Ullah A, Prottoy I, Araf Y, Hossain S, Sarkar B & Saha A, *Comp Mol Biosci*, 9 (2019) 94.
51 Townsend P D, Rodgers T L, Glover L C, Korhonen H J, Richards S A, Colwell L J, Pohl E, Wilson M R, Hodgson D R, McLeish T C & Cann M J, *J Biol Chem*, 290 (2015) 35.
52 Madhumitha H, Ranjani S, Karunyaa R & Hemalatha, S, *Arch Breast Can*, 222 (2023) 231.
53 López-Lázaro M, *Curr Med Chem*, 1324 (2015) 34.
54 Famuyide I M, Aro A O, Fasina F O, Eloff J N & McGaw L J, *BMC Complement Altern Med*, 19 (2019) 141.
55 Chumsri S, Howes T, Bao T, Sabnis G & Brodie A, *J Steroid Biochem Mol Biol*, 13 (2011) 22.
56 Salleh R M, Ong M T & Neda G D, *Int Food Res J*, 20 (2013) 1234.
57 Asysyifa A, Agustiningtyas A & Nurgina I, *Ann Oncology*, 31 (2020) S1266.
58 Geethanjali R, Manjula A C, Mini M & Banu M, *Edu Admin Theory Prac*, 1870 (2024) 1876.
59 Orrantia-Borunda E, Anchondo-Nuñez P, Acuña-Aguilar L E, Gómez-Valles F O & Ramírez-Valdespino CA, *Breast Cancer,* 31 (2022) 42.
60 Atanasov A G, Zotchev S B & Dirsch V M, *Nat Rev Drug Discov*, 200 (2021) 216.
61 Wong R S, *J Exp Clin Cancer Res*, 1 (2011) 14.
62 Bratton S B, MacFarlane M, Cain K & Cohen G M, *Exp Cell Res*, 27 (2000) 33.
63 Yang X H, Sladek T L, Liu X, Butler B R, Froelich C J & Thor A D, *Cancer Res*, 348 (2001) 54.